Editors' Suggestion

Phase Transition to Turbulence via Moving Fronts

Sébastien Gomé,[1,2,*] Aliénor Rivière,[1] Laurette S. Tuckerman,[1] and Dwight Barkley[3]
[1]Laboratoire de Physique et Mécanique des Milieux Hétérogènes, CNRS, ESPCI Paris, PSL Research University, Sorbonne Université, Université Paris-Cité, Paris 75005, France
[2]Department of Physics, Technion Israel Institute of Technology, 32000 Haifa, Israel
[3]Mathematics Institute, University of Warwick, Coventry CV4 7AL, United Kingdom

(Received 13 February 2024; accepted 29 May 2024; published 28 June 2024)

Directed percolation (DP), a universality class of continuous phase transitions, has recently been established as a possible route to turbulence in subcritical wall-bounded flows. In canonical straight pipe or planar flows, the transition occurs via discrete large-scale turbulent structures, known as puffs in pipe flow or bands in planar flows, which either self-replicate or laminarize. However, these processes might not be universal to all subcritical shear flows. Here, we design a numerical experiment that eliminates discrete structures in plane Couette flow and show that it follows a different, simpler transition scenario: turbulence proliferates via expanding fronts and decays via spontaneous creation of laminar zones. We map this phase transition onto a stochastic one-variable system. The level of turbulent fluctuations dictates whether moving-front transition is discontinuous, or continuous and within the DP universality class, with profound implications for other hydrodynamic systems.

DOI: 10.1103/PhysRevLett.132.264002

Landau and Liftshitz [1] describe the subcritical transition to turbulence in shear flows such as pipe and channels as a first-order transition, driven by the competition between two states, one laminar and one turbulent. The stable state invades the metastable state via moving fronts. Below a critical Reynolds number Re_c, laminar flow is the stable asymptotic state. Above Re_c, turbulence is stable and will expand into laminar flow. Pomeau [2] recognized that the problem of subcritical transition is richer than this, since turbulence is a *fluctuating state* and can spontaneously decay to the laminar state, forming *laminar gaps* within turbulence, while laminar flow is an *absorbing state* that cannot spontaneously become turbulent. The subcritical transition to turbulence is thus an absorbing state transition that could be second order and belong to a universality class of nonequilibrium statistical systems known as directed percolation (DP) [3,4].

The apparent simplicity of this story is belied by the multiple-scale structure of transitional turbulence typical in canonical wall-bounded shear flows. At the scales of the wall separation, turbulence consists of streamwise vortices and streaks [5]. At scales an order of magnitude larger, vortices and streaks organize into discrete coherent structures, known as puffs in straight pipe flow or oblique bands in planar flows [6–9]; see Fig. 1(a). To date, all experimental and numerical studies confirming universal DP scaling in wall-bounded flows have shown that bands or puffs control the percolation process [10–15]. This is at odds with the simpler scenario proposed by Pomeau based on front motion, metastability, and laminar gap formation.

Turbulent structures are symbiotically linked to large-scale mean flows [16–23] which dictate both their characteristic size and interactions [24–27]. Large-scale flow energizes turbulent structures [23,26,28] and must be accounted for in theoretical treatments [29–33]. Here, we realize a numerical experiment in which the large-scale flow in plane Couette flow (PCF) is controlled to eliminate the formation of oblique turbulent bands. The resulting flow will be called band-free PCF. With this setup, we investigate the transition to turbulence in a hydrodynamic system without discrete large-scale structures and their associated mean-turbulent coupling.

We use the pseudospectral code CHANNELFLOW [34] to carry out direct numerical simulations (DNS) of the three-dimensional (3D) Navier-Stokes equations governing an incompressible viscous fluid between two parallel rigid plates moving at speeds $\pm U_{\mathrm{wall}}$. Velocities are nondimensionalized by U_{wall}, lengths by the half-gap h between the plates. The Reynolds number is $\mathrm{Re} = hU_{\mathrm{wall}}/\nu$, where ν is the kinematic viscosity. Figure 1(a) shows typical transitional flow containing large-scale oblique turbulent bands. The large-scale flow (arrows) is most pronounced at the interfaces separating turbulent and laminar regions [7,18,19].

The large-scale spanwise velocity is negligible for either fully laminar or fully turbulent flow, but appreciable along turbulent bands. By suppressing it, we seek to eliminate band formation. We introduce streamwise (strm) and spanwise (span) large-scale cutoff wave numbers $(K_{\mathrm{strm}}, K_{\mathrm{span}})$. For Fourier modes $|k_{\mathrm{strm}}| \le K_{\mathrm{strm}}$ and $|k_{\mathrm{span}}| \le K_{\mathrm{span}}$, we set the spanwise velocity to zero while retaining the usual

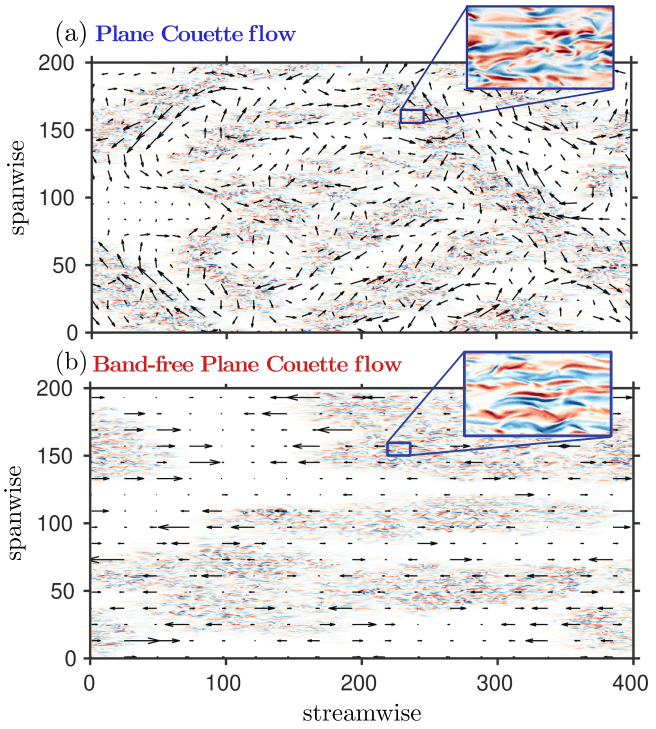

FIG. 1. Visualizations of (a) PCF and (b) band-free PCF at $\mathrm{Re} = 360$ in a domain of size $(L_{\mathrm{strm}}, L_{\mathrm{span}}) = (400, 200)$. Colors show the turbulent fluctuations, visualized via the wall-normal velocity u_y at $y = 0$ (blue: $-0.2 \le u_y < 0$, red: $0 < u_y \le 0.2$). White ($u_y \simeq 0$) signifies quiescent flow. Arrows show the large-scale flow $(u_{\mathrm{strm}}, u_{\mathrm{span}})$. The enlargements of u_y in (a),(b) show the streakiness in the turbulent zones.

momentum equations for streamwise and wall-normal velocity, including incompressibility. This yields a two-component, three-dimensional (2C-3D) hydrodynamic system at large scales. We apply the usual 3D Navier-Stokes equations at small scales, thereby preserving the mechanisms producing wall-bounded turbulence [5,35,36]. The numerical procedure is given in the Supplemental Material [37].

Figure 1(b) displays the flow computed with the cutoff window $(K_{\mathrm{strm}}, K_{\mathrm{span}}) = (0.24, 0.47)$, chosen so that the corresponding wavelengths $(\Lambda_{\mathrm{strm}}, \Lambda_{\mathrm{span}}) \simeq (26, 13)$ are smaller than the typical wavelengths $(\lambda_{\mathrm{strm}}, \lambda_{\mathrm{span}}) \simeq (100, 44)$ of the turbulent bands in PCF [7]. The large-scale flow is streamwise oriented by construction. Our procedure has the desired effect of eliminating the turbulent bands—the laminar-turbulent interfaces do not have the well-defined angles and widths seen in Fig. 1(a).

In order to study spatiotemporal dynamics, we perform simulations in a long slender domain tilted with respect to the streamwise direction by $\theta = 24°$, a typical angle at which bands occur; see Refs. [7,8]. We denote the slender direction parallel to the bands by x and the long direction perpendicular to them by z. This geometry has been shown to capture important features of turbulent bands while reducing their behavior to quasi-1D dynamics along z [8,10,18,45,46]. For consistency and comparison, we use the same domain for band-free PCF, in which we suppress large-scale *spanwise* velocity (see Supplemental Material [37], Sec. IB).

Mean-turbulent interaction.—Prior to comparing the transition scenarios in PCF and band-free PCF, we focus on the coupling between turbulence and large-scale mean flow. We decompose the velocity $\boldsymbol{u} = \bar{\boldsymbol{u}} + \boldsymbol{u}'$, where averages $\overline{(\cdot)}$ are taken over x and time periods during which turbulent fronts are approximately stationary. The turbulent kinetic energy $E_{\mathrm{turb}} \equiv \frac{1}{2}\overline{\boldsymbol{u}' \cdot \boldsymbol{u}'}$ and the mean streamwise velocity $\bar{u}_{\mathrm{strm}}$ are plotted in Fig. 2.

The significant difference between PCF and band-free PCF is in the spatial phase relation between E_{turb} and $\bar{u}_{\mathrm{strm}}$, seen at $y = 0.5$ in Figs. 2(b) and 2(d). (Reflected plots would be obtained at $y = -0.5$.) Turbulence extracts energy from the local mean shear, thereby flattening the profile and reducing $\bar{u}_{\mathrm{strm}}$ at $y = 0.5$. For bands in PCF, advection by the large-scale flow (arrows) redistributes momentum and energy from laminar to turbulent regions [18] (see especially Fig. 6(b) in [28]). It is the competing mechanisms of mean-flow flattening by turbulence and mean flow fueling nearby turbulence that are encrypted in the phase relation between $\bar{u}_{\mathrm{strm}}$ and E_{turb} [see Fig. 2(e)]. When turbulence is *excited* [E_{turb} increases, see Fig. 2(b)], it is first fueled by the large-scale flow. Hence, $\bar{u}_{\mathrm{strm}}$ does not react directly to it and decreases only after a phase shift, and then vice versa in the *refractory* region.

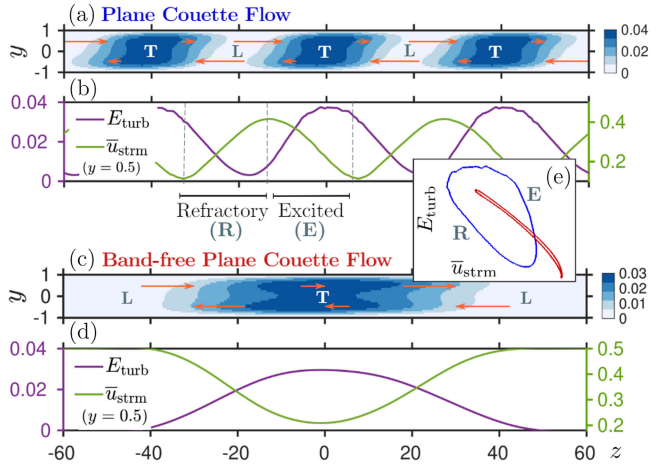

FIG. 2. Turbulent kinetic energy E_{turb} and mean streamwise velocity $\bar{u}_{\mathrm{strm}}$ in (a),(b) PCF and (c),(d) band-free PCF. Contour plots (a),(c) show $E_{\mathrm{turb}}(y, z)$ and arrows show $\bar{u}_{\mathrm{strm}}(\pm 0.5, z)$ Unlike in (a), turbulent zones in (c) do not have a selected width. Curves in (b,d) show E_{turb} and $\bar{u}_{\mathrm{strm}}$ as a function of z at $y = 0.5$. (e) Phase-plane representation of $\bar{u}_{\mathrm{strm}}$ and E_{turb} at $y = 0.5$ in PCF (blue) and band-free PCF (red). In contrast to PCF, turbulence and mean-flow in band-free PCF are in phase. Abbreviations: laminar (L); turbulent (T); refractory (R); excited (E).

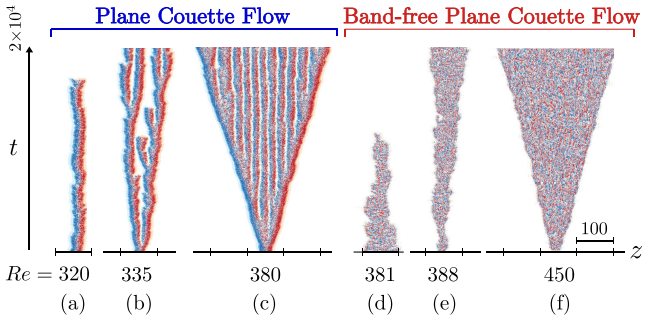

FIG. 3. Band and slug regimes in (a),(b),(c) PCF and (d),(e),(f) band-free PCF initiated from a turbulent patch. Colors show the spanwise velocity u_{span} at $y = 0$, $x = 0$ as a function of z and t (blue: $-0.1 \le u_{\text{span}} \le 0$, red: $0 \le u_{\text{span}} \le 0.1$). The wide blue and red areas visible in PCF result from the large-scale flow.

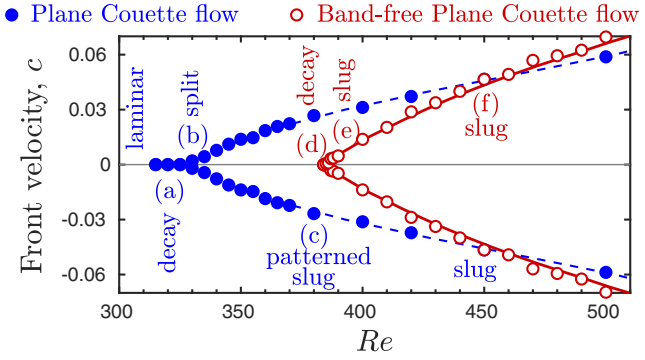

FIG. 4. Front velocity as a function of Re in both PCF and band-free PCF. Labels (a)–(f) correspond to the visualizations of Fig. 3(a)–3(f). The points of zero propagation speed are $\text{Re}_0 \simeq 325$ for PCF [45] and $\text{Re}_0 \simeq 383$ for band-free PCF. Speeds below Re_0 in band-free PCF are not shown; see Supplemental Material [37]. The blue curve guides the eye, while the continuous red curves come from simulations of model (1).

Excited and refractory regions are essential for sustaining localized turbulent regions and for their duplication and interactions [23–25,30].

In band-free PCF, we find that turbulence and mean flow are not phase shifted and excited and refractory zones are absent, i.e., E_{turb} is a single-valued function of $\bar{u}_{\text{strm}}$ [Fig. 2(e)]. This follows from the approximate z-reflection symmetry apparent in Figs. 2(c) and 2(d) (see Supplemental Material [37], Sec. ID). This has major consequences for the way that turbulence emerges in this flow.

Transition with and without bands.—Transition scenarios in PCF and in band-free PCF are illustrated by spatiotemporal diagrams in Fig. 3. Each simulation is initiated with a localized turbulent patch.

The scenario for PCF is well documented in this geometry [8,10,27,45]. Below $\text{Re} \simeq 350$, turbulent bands are localized metastable structures that survive for long times before decaying [Fig. 3(a)] or proliferating by splitting [Fig. 3(b)] [45]. Decay and splitting are memoryless processes, in that their associated waiting times are exponentially distributed. Above $\text{Re}_0 \simeq 325$ [45], the proliferation of a single band becomes more probable than its decay, and turbulence survives, albeit in intermittent form [10,13]. In the thermodynamic limit of large systems with many bands and long times, this intermittency gives rise to a critical point in the DP universality class at the estimated critical value $\text{Re}_c = 328.7$ [10,13]. (Re_c and Re_0 are close, but distinctly different: Re_0 is determined from single isolated bands while Re_c is influenced by interactions between bands.) For $\text{Re} \gtrsim 350$, e.g., Fig. 3(c), turbulence proliferates via expanding fronts moving at equal and opposite speeds (*slug* phase [30]). The mean left-going and right-going front propagation speeds are shown in Fig. 4. Below $\text{Re} \simeq 450$, the fronts delimit a nearly periodic interior pattern [Fig. 3(c)] [45], which is absent above $\text{Re} \simeq 450$ (not shown).

By design, band-free PCF does not exhibit discrete turbulent structures or patterns. Turbulence contracts and expands, not via decay and splitting of discrete structures, but rather via fluctuating front motion, shown in Figs. 3(d)–3(f), whose expansion speeds are also shown in Fig. 4. Importantly, the decay of turbulence is not a memoryless process because the mean lifetime of a patch depends on its initial size, unlike in PCF and pipe flow [11,45,47], but like low-Re plane channel flow [48,49].

Figures 5(a) and 5(b) shows the spatiotemporal dynamics from a fully turbulent initial state in a long domain below ($\text{Re} = 370$) and above ($\text{Re} = 385$) the critical point Re_c in band-free PCF. Laminar gaps nucleate within the turbulent flow and interfaces fluctuate. Below Re_c, turbulence predominantly contracts and asymptotically the flow is laminar. Above Re_c, laminar gaps are created but eventually close as a consequence of preferred turbulent expansion.

The order parameter for the transition is the equilibrium turbulent fraction, F_t, which is the mean proportion of turbulent flow at statistical equilibrium (see Supplemental Material [37]). F_t is plotted as a function of Re in Fig. 5(c) for both PCF [10] and band-free PCF. For comparison, we use reduced Reynolds numbers, $\epsilon \equiv (\text{Re} - \text{Re}_c)/\text{Re}_c$. For PCF, $\text{Re}_c \simeq 328.7$ [10]. For band-free PCF we estimate $\text{Re}_c \simeq 383.5$. Without bands, the transition to uniform turbulence occurs over a significantly shorter range of Re ($F_t \simeq 0.9$ at $\epsilon \simeq 0.01$, while $F_t \simeq 0.2$ at $\epsilon \simeq 0.01$ in PCF).

Measuring F_t near $\epsilon = 0$ is exceedingly costly because scales diverge and hence simulations become susceptible to finite-size, finite-time effects. We have not attempted to determine critical scalings associated with transition in band-free PCF.

A model for percolation via front motion.—Published models for puffs and bands contain at least two fields [29–33]; two are necessary to capture the interaction between mean-flow and turbulence responsible for discrete structures; see Figs. 2(a) and 2(b). Band-free PCF lacks

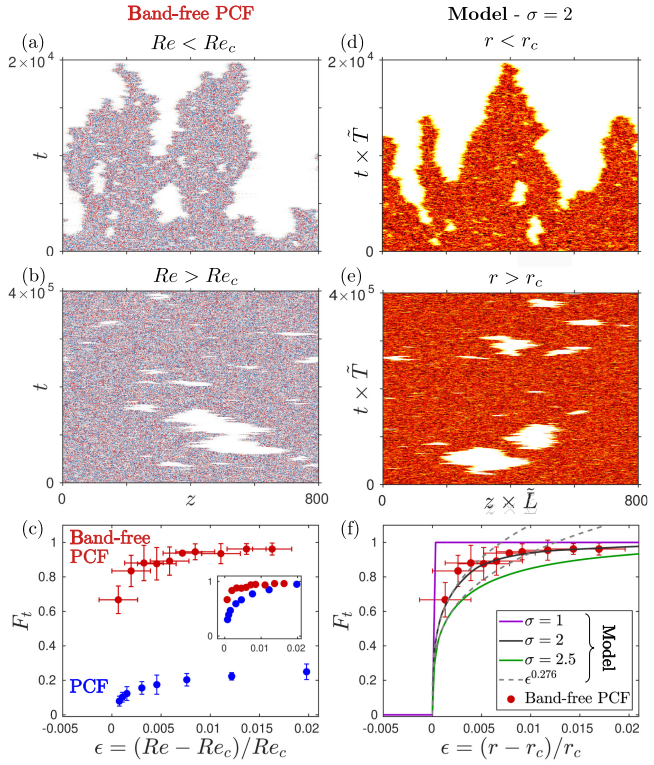

FIG. 5. Laminar-turbulent percolation in band-free PCF at (a) $\mathrm{Re} = 370 < \mathrm{Re}_c$ and (b) $\mathrm{Re} = 385 > \mathrm{Re}_c$. (c) Equilibrium turbulent fraction F_t as a function of $\epsilon \equiv (\mathrm{Re} - \mathrm{Re}_c)/\mathrm{Re}_c$ in PCF (blue, data from Ref. [10]) and band-free PCF (red). The inset in (c) shows PCF data rescaled by $F_t(\epsilon = 0.02)$ and confirms the more abrupt transition in band-free PCF. (d),(e) Space-time visualization of model (1) with $\sigma = 2.0$ at (d) $r < r_c \simeq 0.2517$ and (e) $r > r_c$. Time and length in the model are rescaled with $\tilde{T}$ and $\tilde{L}$, and r values are chosen such that $r - r_0 = b\mathrm{Re} - \mathrm{Re}_0)$. (f) Same as (c) for model (1) with $\sigma = 1.0$ (first-order), 2.0, and 2.5 (both second-order cases exhibiting DP scaling $\epsilon^{0.276}$, see dashed lines).

discrete structures and mean flow and turbulence are slaved, see Figs. 2(c) and 2(d). This suggests modeling band-free PCF with a single scalar field $q(z, t)$ representing the local turbulent energy.

Following [2,30,50], we consider the stochastic model

$$\partial_t q = \partial_z^2 q - \partial_q V + \sigma q \xi, \tag{1}$$

with the double-well potential

$$V(q) \equiv \frac{q^2}{2}\left[1 + (r+1)\left(\frac{q^2}{2} - \frac{4q}{3}\right)\right],$$

ξ a space-time Gaussian white noise of unit variance and σ a parameter controlling the noise strength. Parameter r plays the role of Re. V has one local minimum at $q = 0$ (laminar) and one at $q > 0$ (turbulent state), the latter being the lowest minimum for $r > 1/8$. Multiplicative noise $\sigma q \xi$ represents turbulent fluctuations and vanishes at $q = 0$, making it an absorbing state; see Refs. [51–53]. Hence model (1) describes fronts between an absorbing and a fluctuating state, just as Pomeau originally envisioned for the transition to turbulence [2,30,50].

We solve (1) via a finite-difference scheme under the Itô representation [54]. We first simulate expanding slugs. Front velocities are found to closely obey the self-similar expression $c \simeq F[r - r_0(\sigma)]$ where $F(0) = 0$ and $r_0(\sigma) \simeq 1/8 + 3\sigma^2/100$. F is independent of σ. Front speeds in band-free PCF, shown in Fig. 4, follow $c_{\mathrm{DNS}} \simeq aF[b(\mathrm{Re} - \mathrm{Re}_0)]$ (solid red line), where a and b rescale velocities and Re, respectively. The agreement is excellent.

The fit of the model speeds to those of band-free PCF establishes the correspondence between r and Re. We determine the ratio $\tilde{L} \simeq 3.0$ of band-free PCF to model length scales from the width of laminar-turbulent fronts. From $\tilde{L}$ and a, we obtain a ratio of time scales between band-free PCF and model, $\tilde{T} = \tilde{L}/a \simeq 16$ (see Supplemental Material [37]). The final model parameter σ is chosen so as to reproduce the phenomenology of band-free PCF as we now show.

With $\sigma = 2.0$, simulations of (1) with space, time and Re rescaling are visualized in Figs. 5(d) and 5(e). The model closely reproduces the dynamics of fluctuating fronts and the nucleation of laminar gaps within turbulent flow as seen in band-free PCF [Figs. 5(a) and 5(b)].

The noise intensity σ indirectly controls the rate of laminar-gap nucleation, and, consequently, the order of the phase transition, as we show in Fig. 5(f). With sufficiently strong noise ($\sigma = 2.0$ and 2.5), the transition is continuous and exhibits the scalings of DP ($F_t \sim \epsilon^{0.276}$, spatial and temporal correlations $\xi_\perp \sim \epsilon^{1.097}$ and $\xi_\parallel \sim \epsilon^{1.734}$; see Supplemental Material [37]). Meanwhile, at low noise ($\sigma = 1.0$) the transition is discontinuous, with no intermediate $0 < F_t < 1$ sustained. The transition becomes sharper as σ is decreased.

We find that the value $\sigma = 2.0$ captures the dependence of turbulent fraction on Re in band-free PCF [Fig. 5(f)] with similar sharp increase in F_t, and specifically gives $F_t(\epsilon \simeq 0.01) \simeq 0.9$. (The accuracy of this match is limited by the precision of Re_c.) Because this value of σ corresponds to a continuous phase transition, this strongly suggests that band-free PCF, like PCF, undergoes a continuous transition in the DP universality class.

Conclusion and discussion.—In subcritical shear flows, turbulence appears, not by increasing its intensity, but by occupying an increasing proportion of space as Reynolds number is increased. In previous studies of canonical straight pipe or planar flows, transition occurs via the percolation of discrete turbulent structures that individually decay or self-replicate. Large-scale mean flow plays a crucial role in these systems by selecting these discrete structures.

Here, we investigate a plane-Couette setup without discrete structures. Transition follows a distinctly different

scenario, mediated by expanding turbulent fronts and spontaneous nucleation of laminar gaps. The observed dynamics are very well captured by a simple stochastic, double-well model with a single field. The order of this phase transition is governed by the nucleation rate of laminar gaps, which depends on the level of fluctuations.

This front-moving transition should be pervasive in systems where discrete puffs or bands are absent. Numerous flows, such as bent pipes [55], body-forced pipes [56], stably-stratified flows [57], suction boundary layer [58], or constrained Couette flow [59,60], lack discrete turbulent structures and may follow this scenario. Our Letter suggests that in such flows, the level of turbulent fluctuations plays a crucial role in dictating whether front-moving transition is first order, as recently reported in experiments of curved and body-forced pipes [56], or second-order and within the DP universality class.

We thank Anna Frishman, Yohann Duguet, Santiago Benavides, François Pétrélis, and Tobias Grafke for fruitful discussions. The calculations for this work were performed using high performance computing resources provided by the Grand Equipement National de Calcul Intensif at the Institut du Développement et des Ressources en Informatique Scientifique (IDRIS, CNRS) through Grant No. A0142A01119. This work was partly supported by a grant from the Simons Foundation (Grant No. 662985, D. B. and L. S. T.).

*Contact author: sebastien.gome@gmail.com

[1] L. D. Landau and E. M. Lifshitz, *Fluid Mechanics: Course of Theoretical Physics, Volume 6*, 2nd ed. (Butterworth-Heinemann, London, 1987).
[2] Y. Pomeau, Front motion, metastability and subcritical bifurcations in hydrodynamics, Physica (Amsterdam) **23D**, 3 (1986).
[3] P. Grassberger, On phase transitions in Schlögl's second model, in *Nonlinear Phenomena in Chemical Dynamics* (Springer, New York, 1981), p. 262.
[4] H.-K. Janssen, On the nonequilibrium phase transition in reaction-diffusion systems with an absorbing stationary state, Z. Phys. B **42**, 151 (1981).
[5] F. Waleffe, On a self-sustaining process in shear flows, Phys. Fluids **9**, 883 (1997).
[6] A. Prigent, G. Grégoire, H. Chaté, O. Dauchot, and W. van Saarloos, Large-scale finite-wavelength modulation within turbulent shear flows, Phys. Rev. Lett. **89**, 014501 (2002).
[7] A. Prigent, G. Grégoire, H. Chaté, and O. Dauchot, Long-wavelength modulation of turbulent shear flows, Physica (Amsterdam) **174D**, 100 (2003).
[8] D. Barkley and L. S. Tuckerman, Computational study of turbulent-laminar patterns in Couette flow, Phys. Rev. Lett. **94**, 014502 (2005).
[9] Y. Duguet, P. Schlatter, and D. S. Henningson, Formation of turbulent patterns near the onset of transition in plane Couette flow, J. Fluid Mech. **650**, 119 (2010).
[10] G. Lemoult, L. Shi, K. Avila, S. V. Jalikop, M. Avila, and B. Hof, Directed percolation phase transition to sustained turbulence in Couette flow, Nat. Phys. **12**, 254 (2016).
[11] K. Avila, D. Moxey, A. de Lozar, M. Avila, D. Barkley, and B. Hof, The onset of turbulence in pipe flow, Science **333**, 192 (2011).
[12] M. Chantry, L. S. Tuckerman, and D. Barkley, Universal continuous transition to turbulence in a planar shear flow, J. Fluid Mech. **824**, R1 (2017).
[13] L. Klotz, G. Lemoult, K. Avila, and B. Hof, Phase transition to turbulence in spatially extended shear flows, Phys. Rev. Lett. **128**, 014502 (2022).
[14] K. Takeda, Y. Duguet, and T. Tsukahara, Intermittency and critical scaling in annular Couette flow, Entropy **22**, 988 (2020).
[15] K. Kohyama, M. Sano, and T. Tsukahara, Sidewall effect on turbulent band in subcritical transition of high-aspect-ratio duct flow, Phys. Fluids **34**, 084112 (2022).
[16] D. Coles and C. van Atta, Progress report on a digital experiment in spiral turbulence, AIAA J. **4**, 1969 (1966).
[17] I. J. Wygnanski and F. Champagne, On transition in a pipe. Part 1. The origin of puffs and slugs and the flow in a turbulent slug, J. Fluid Mech. **59**, 281 (1973).
[18] D. Barkley and L. S. Tuckerman, Mean flow of turbulent–laminar patterns in plane Couette flow, J. Fluid Mech. **576**, 109 (2007).
[19] Y. Duguet and P. Schlatter, Oblique laminar-turbulent interfaces in plane shear flows, Phys. Rev. Lett. **110**, 034502 (2013).
[20] M. Couliou and R. Monchaux, Large-scale flows in transitional plane Couette flow: A key ingredient of the spot growth mechanism, Phys. Fluids **27**, 034101 (2015).
[21] L. Klotz, A. Pavlenko, and J. Wesfreid, Experimental measurements in plane Couette-Poiseuille flow: Dynamics of the large- and small-scale flow, J. Fluid Mech. **912** (2021).
[22] E. Marensi, G. Yalnız, and B. Hof, Dynamics and proliferation of turbulent stripes in plane-Poiseuille and plane-Couette flows, J. Fluid Mech. **974**, A21 (2023).
[23] C. W. van Doorne and J. Westerweel, The flow structure of a puff, Phil. Trans. R. Soc. A **367**, 489 (2009).
[24] B. Hof, A. De Lozar, M. Avila, X. Tu, and T. M. Schneider, Eliminating turbulence in spatially intermittent flows, Science **327**, 1491 (2010).
[25] D. Samanta, A. De Lozar, and B. Hof, Experimental investigation of laminar turbulent intermittency in pipe flow, J. Fluid Mech. **681**, 193 (2011).
[26] B. Song, D. Barkley, B. Hof, and M. Avila, Speed and structure of turbulent fronts in pipe flow, J. Fluid Mech. **813**, 1045 (2017).
[27] S. Gomé, L. S. Tuckerman, and D. Barkley, Patterns in transitional shear turbulence. Part 2. Emergence and optimal wavelength, J. Fluid Mech. **964**, A17 (2023).
[28] S. Gomé, L. S. Tuckerman, and D. Barkley, Patterns in transitional shear turbulence. Part 1. Energy transfer and mean-flow interaction, J. Fluid Mech. **964**, A16 (2023).
[29] D. Barkley, Simplifying the complexity of pipe flow, Phys. Rev. E **84**, 016309 (2011).
[30] D. Barkley, Theoretical perspective on the route to turbulence in a pipe, J. Fluid Mech. **803**, P1 (2016).

[31] S. J. Benavides and D. Barkley, Model for transitional turbulence in a planar shear flow, arXiv:2309.12879.
[32] D. Barkley, Modeling the transition to turbulence in shear flows, J. Phys. Conf. Ser. **318**, 032001 (2011).
[33] X. Wang, H.-Y. Shih, and N. Goldenfeld, Stochastic model for quasi-one-dimensional transitional turbulence with streamwise shear interactions, Phys. Rev. Lett. **129**, 034501 (2022).
[34] J. Gibson, F. Reetz, S. Azimi, A. Ferraro, T. Kreilos, H. Schrobsdorff, M. Farano, A. Yesil, S. Schütz, M. Culpo, and T. Schneider, Channelflow 2.0 (to be published), see channelflow.ch.
[35] J. M. Hamilton, J. Kim, and F. Waleffe, Regeneration mechanisms of near-wall turbulence structures, J. Fluid Mech. **287**, 317 (1995).
[36] T. Liu, B. Semin, R. Godoy-Diana, and J. E. Wesfreid, Lift-up and streak waviness drive the self-sustained process in wall-bounded transition to turbulence, Phys. Rev. Fluids **9**, 033901 (2024).
[37] See Supplemental Material at http://link.aps.org/supplemental/10.1103/PhysRevLett.132.264002, which includes Refs. [38–44] for numerical methods and additional information on model (1) and Figs. 2, 4, and 5.
[38] C. Canuto, M. Y. Hussaini, A. Quarteroni, and T. A. Zang, *Spectral Methods: Fundamentals in Single Domains* (Springer-Verlag, Berlin Heidelberg, 2007).
[39] J. Jiménez and A. Pinelli, The autonomous cycle of near-wall turbulence, J. Fluid Mech. **389**, 335 (1999).
[40] J. Jimenez, Streak-less wall-bounded turbulence, arXiv:2202.09814.
[41] A. Lundbladh and A. V. Johansson, Direct simulation of turbulent spots in plane Couette flow, J. Fluid Mech. **229**, 499 (1991).
[42] W. Van Saarloos, Front propagation into unstable states, Phys. Rep. **386**, 29 (2003).
[43] H. Hinrichsen, Non-equilibrium critical phenomena and phase transitions into absorbing states, Adv. Phys. **49**, 815 (2000).
[44] S. Lübeck, Universal scaling behavior of non-equilibrium phase transitions, Int. J. Mod. Phys. B **18**, 3977 (2004).
[45] L. Shi, M. Avila, and B. Hof, Scale invariance at the onset of turbulence in Couette flow, Phys. Rev. Lett. **110**, 204502 (2013).
[46] S. Gomé, L. S. Tuckerman, and D. Barkley, Statistical transition to turbulence in plane channel flow, Phys. Rev. Fluids **5**, 083905 (2020).
[47] M. Avila, A. P. Willis, and B. Hof, On the transient nature of localized pipe flow turbulence, J. Fluid Mech. **646**, 127 (2010).
[48] V. Mukund, C. Paranjape, M. P. Sitte, and B. Hof, Aging and memory of transitional turbulence, arXiv:2112.06537.
[49] D. Xu and B. Song, Size-dependent transient nature of localized turbulence in transitional channel flow, J. Fluid Mech. **950**, R3 (2022).
[50] Y. Pomeau, The transition to turbulence in parallel flows: A personal view, C. R. Méc. **343**, 210 (2015).
[51] M. A. Munoz, Nature of different types of absorbing states, Phys. Rev. E **57**, 1377 (1998).
[52] M. A. Munoz and R. Pastor-Satorras, Stochastic theory of synchronization transitions in extended systems, Phys. Rev. Lett. **90**, 204101 (2003).
[53] M. A. Munoz, Multiplicative noise in non-equilibrium phase transitions: A tutorial, arXiv:cond-mat/0303650.
[54] C. W. Gardiner, *Handbook of Stochastic Methods* (Springer, Berlin, 1985), Vol. 3.
[55] E. Rinaldi, J. Canton, and P. Schlatter, The vanishing of strong turbulent fronts in bent pipes, J. Fluid Mech. **866**, 487 (2019).
[56] Y. Zhuang, B. Yang, V. Mukund, E. Marensi, and B. Hof, Discontinuous transition to shear flow turbulence, arXiv:2311.11474.
[57] C. Rorai, P. D. Mininni, and A. Pouquet, Turbulence comes in bursts in stably stratified flows, Phys. Rev. E **89**, 043002 (2014).
[58] T. Khapko, P. Schlatter, Y. Duguet, and D. S. Henningson, Turbulence collapse in a suction boundary layer, J. Fluid Mech. **795**, 356 (2016).
[59] Y. Duguet, O. Le Maitre, and P. Schlatter, Stochastic and deterministic motion of a laminar-turbulent front in a spanwisely extended Couette flow, Phys. Rev. E **84**, 066315 (2011).
[60] A. Pershin, C. Beaume, and S. M. Tobias, Dynamics of spatially localized states in transitional plane Couette flow, J. Fluid Mech. **867**, 414 (2019).